This is an open access article published under an ACS AuthorChoice License, which permits copying and redistribution of the article or any adaptations for non-commercial purposes.

ACS OMEGA

http://pubs.acs.org/journal/acsodf

Article

# Computer Test of a Modified Silicene/Graphite Anode for Lithium-Ion Batteries

Alexander Y. Galashev,* Ksenia A. Ivanichkina, Konstantin P. Katin, and Mikhail M. Maslov

Cite This: *ACS Omega* 2020, 5, 13207−13218

Read Online

ACCESS | Metrics & More | Article Recommendations | Supporting Information

**ABSTRACT:** Despite the considerable efforts made to use silicon anodes and composites based on them in lithium-ion batteries, it is still not possible to overcome the difficulties associated with low conductivity, a decrease in the bulk energy density, and side reactions. In the present work, a new design of an electrochemical cell, whose anode is made in the form of silicene on a graphite substrate, is presented. The whole system was subjected to transmutation neutron doping. The molecular dynamics method was used to study the intercalation and deintercalation of lithium in a phosphorus-doped silicene channel. The maximum uniform filling of the channel with lithium is achieved at 3% and 6% P-doping of silicene. The high mobility of Li atoms in the channel creates the prerequisites for the fast charging of the battery. The method of statistical geometry revealed the irregular nature of the packing of lithium atoms in the channel. Stresses in the channel walls arising during its maximum filling with lithium are significantly inferior to the tensile strength even in the presence of polyvacancies in doped silicene. The proposed design of the electrochemical cell is safe to operate.

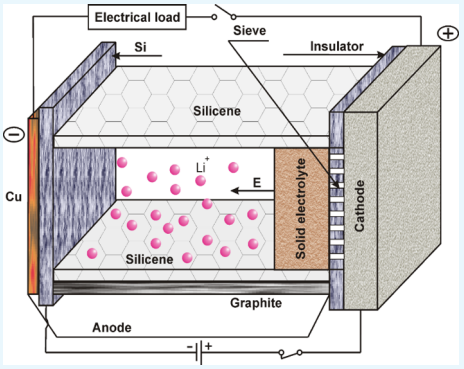


Downloaded via 213.142.35.54 on September 28, 2020 at 08:44:12 (UTC).
See https://pubs.acs.org/sharingguidelines for options on how to legitimately share published articles.

## INTRODUCTION

Understanding the relationship between the atomic interaction of lithium with two-dimensional (2D) materials and the electrochemical properties they exhibit is important for optimizing the performance and design of next-generation lithium-ion current sources.[1−3] One of the main problems for creating a high-power lithium-ion battery (LIB) is finding a material for its anode. When selecting an anode material for LIB, it is first of all taken into account how much lithium this material can contain during the intercalation of this alkali metal. According to this criterion, the best materials for the anode are silicon and tin. In either case, up to 4.4 Li atoms can fall per atom of a selected material (Si or Sn). However, silicon is still preferred here because of its higher thermal and mechanical strength. Indeed, the melting temperature of silicon (1411 °C) is 6 times higher than that of tin, and the tensile strength and yield strength of Si are on an average higher than that of Sn by 3.5 and 5.8 times, respectively. In addition, above 161 °C, tin becomes brittle and can be easily pulverized, and at temperatures lower than 13.2 °C, white tin transitions to gray tin. At the same time, the specific volume of the metal increases by 25.6%, which creates the conditions for tin scattering. Thus, silicon is the number one contender for the manufacture of the LIB anode. However, bulk silicon is not suitable for this purpose because of the large increase in volume (up to 400%) during the intercalation of lithium. After a small number of cycles, such anode material is destroyed.[4] The use of a composite material from graphene and silicon nanoparticles is also not entirely successful because of the loss of adhesion between them during intercalation/deintercalation.[5]

The main problem for creating high-capacity and high-power LIBs is to find a suitable anode material that would constitute an alternative to graphite, which is currently used for this purpose.[6] Of all the materials tested, silicon is the most suitable candidate for use as the anode material. The theoretical specific capacity of silicon is extremely high (4200 mA h/g). However, both crystalline and amorphous silicon turned out to be unsuitable anode materials because of the low resistance to cycling.

The situation is corrected when using 2D silicon or silicene as the anode material. The binding energy between Si atoms in silicene and Li atoms is quite high. This, along with a low barrier to the diffusion of lithium atoms in silicene, the production of high energy density, a significantly lower volume change, and increased stability during cycling, makes silicene a promising anode material.[4]

In order to use silicene as an anode material, some established facts should be taken into account. Because of the metastable nature of silicene, it needs to be stabilized on

Received: March 20, 2020
Accepted: May 15, 2020
Published: May 28, 2020

ACS Publications

© 2020 American Chemical Society

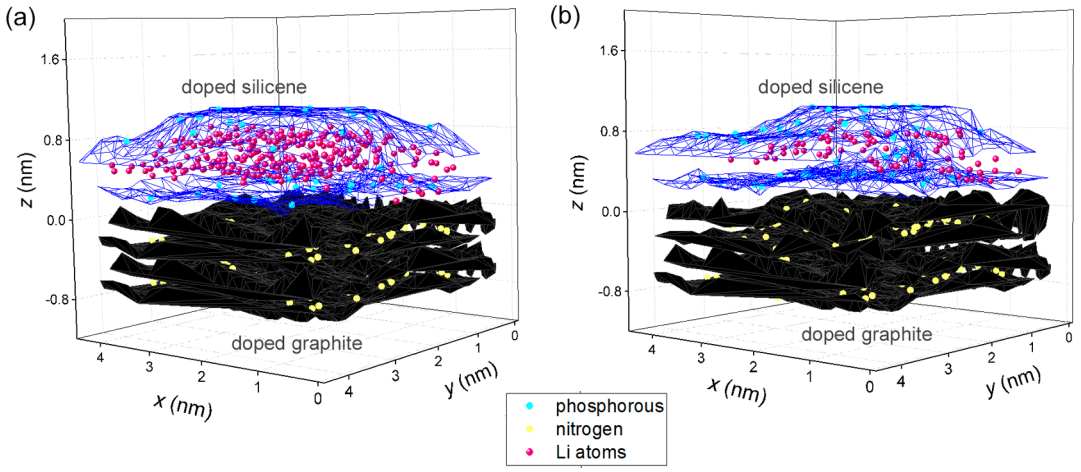


**Figure 1.** Lithium-filled silicene channel with a gap of 0.24 nm between the sheets after 500 ps for (a) 6% doped silicene and (b) 9% doped silicene.

the substrate and out of the vacuum.[7] A strict choice of substrate is necessary because it will be used in the future together with silicene. Silicene in the presence of air spontaneously oxidizes. Therefore, it is proposed to cover it with a protective $Al_2O_3$ film for further use.[8] The accelerated method of ab initio calculation of free energy allows to some extent to predict the optimal conditions for the growth of new 2D materials.[9] There is an indication that multilayer silicene grown on an Ag(111) substrate exhibits a number of properties of a single-layer freestanding silicone.[10] In particular, Dirac fermions are present in it. However, in a single-layer silicene on metal (Ir, Cu, Mg, Au, Pt, Al, and Ag) substrates, the Dirac cone disappears,[11] although the creation of an alkali metal layer between the substrate and silicene restores it. Pentasilicene, such as ordinary hexagonal silicene, has low diffusion barriers for $Li^+$ ions.[12] During lithium adsorption, a transition from a semiconductor to a metal occurs in it. It is expected that its use as an anode material will result in an ultrafast charge/discharge rate. Freestanding silicene is characterized by higher tensile strength (12.5 GPa) than bulk silicon (5.7 GPa).[13] Modeling the filling of nine-layer silicene with lithium revealed less destruction of this material during vertical (perpendicular to the plane of silicene sheets) penetration of Li atoms compared to horizontal (parallel to the plane of sheets) penetration.[14] The presence of mono- and bivacancies in silicene markedly reduced the barrier accompanying the entry of Li atoms into the silicon-layered material regardless of its orientation to the atomic flux. Density functional theory (DFT) calculations of lithium adsorption on a single-layer silicene predict the production of a capacity of 1196 mA h $g^{-1}$ for a silicene anode without breaking Si−Si bonds.[15] The charge capacity of a freestanding two-layer silicene during intercalation of lithium can reach 1384 mA h $g^{-1}$.[16]

After the discovery of silicene,[17] that is, a 2D single-layer silicon with a hexagonal cellular structure, it became possible to create a LIB anode that meets the necessary conditions for maintaining a high charge capacity and withstanding a significant number of LIB charge/discharge cycles. A detailed computer study of the functioning of a silicene anode using metal (Ag, Al, Cu, and Ni) and graphite substrates was carried out in.[18−23] These studies have shown the fundamental possibility of using such anodes. However, their disadvantages were also revealed; in particular, this relates to the mechanical properties of defective silicene. It was shown that the presence of mono- and bivacancies in silicene could significantly increase the charging capacity of the electrode, whereas, with larger defects, silicene exhibits mechanical instability during the intercalation of lithium. In addition, buckles on silicene supported by metal substrates increase, which decrease the filling of channels formed by it with lithium.

Freestanding silicene is a narrow-gap semiconductor with a band gap of about 27 meV.[24] The low electrical conductivity of this material should manifest itself at a low rate of charging and discharging LIBs. However, silicene on the substrate is able to change its electronic properties significantly; in particular, it can turn into a conductive material.[25] In an experimental study of strong doping with phosphorus, silicon showed that the strength of the Si−P bond is higher than that of the Si−Si bond.[26] In order to improve the quality of the anode material, the silicene used to create it must be modified. The mechanical properties of silicene should be strengthened, and its electrical conductivity is increased. We suggested that the simultaneous solution of both of these problems could be achieved by doping silicene with phosphorus.

The electronic properties of a semiconductor can be improved by doping. Natural silicon atoms consist of three isotopes, $^{28}Si$ (abundance 92.23%), $^{29}Si$ (abundance: 4.67%), and $^{30}Si$ (abundance: 3.10%). The capture of thermal neutrons by the $^{30}Si$ isotope leads to the unstable $^{31}Si$ isotope undergoing beta decay. As a result of this decay, a $^{31}P$ phosphorus atom is formed. This indicates that an n-type impurity doping occurs in the silicon material. Without taking into account the emission of antineutrinos, this process is presented in the form of a chain of reactions

$$^{30}Si + n \rightarrow {}^{31}Si \rightarrow (\beta^-)^{31}P \quad (1)$$

Thus, as a result of the irradiation of silicon with thermal neutrons, only one complete nuclear reaction occurs. Moreover, the half-life of $^{31}Si$ is only 2.62 h. Because of this fact, the NTD method has found wide applications on an industrial scale. Silicon still plays a key role in the creation of electronic devices. Silicon matrices require alloying to obtain functional elements of electronics. The conductivity of semiconductors is ensured by both electrons transferred from the valence band to the conduction band and holes left by electrons in the valence band. The mobility of both of these charges creates the real conductivity of the material. As a result of doping with a group V element, one of the dopant electrons in silicon is not bound


https://dx.doi.org/10.1021/acsomega.0c01240
ACS Omega 2020, 5, 13207−13218

by a covalent bond and can freely migrate along the crystal lattice. Moreover, it does not leave holes in the valence band. In this case, electrons are the main charge carriers.

The goal of this work is a computer study of intercalation and deintercalation of lithium into a silicene channel on a graphite substrate after irradiation of this system with thermal neutrons, that is, in the presence of doping atoms of phosphorus and nitrogen in the corresponding subsystems.

## RESULTS AND DISCUSSION

The general view of the LIB is presented in Figure 12 in the "Computational Methods" section. The calculation showed that an increase in doping degree leads to greater distortion of silicene sheets (Figure 1). In the case when silicene contained only 6% of phosphorus dopant, the top sheet of graphite and both sheets of silicene have a fairly flat shape. Almost straight walls of the channel contribute to its filling. The channel is filled with 271 lithium atoms. The upper and lower front edges of the channel, as well as the corresponding edges at the outlet of the channel, are slightly moved toward each other. This, to some extent, prevents the escape of Li atoms from the channel. When silicene contained 9% dopant, the phosphorus atoms formed clusters outside the vacancy defects, which turned out to be open. This circumstance leads to the loosening of the channel walls. In this case, the distortion of the silicene channel makes it difficult to move lithium further along the channel, and the maximum possible number of intercalated Li atoms is only 71.

To show the difference in the results of the intercalation of lithium in silicene channels with different gaps, shown in Figure 2, we compare the results of filling nonirradiated

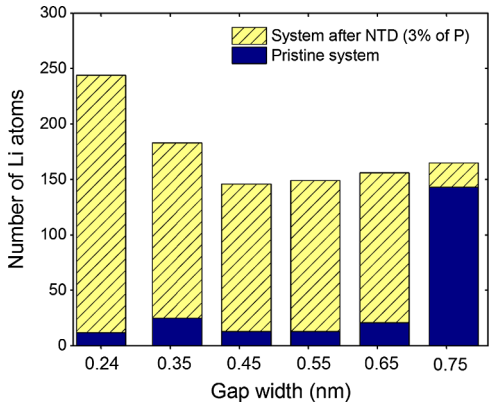


**Figure 2.** Maximum number of lithium atoms obtained as a result of intercalation in undoped and 3% P-doped silicene channels depending on the gap width $h_g$ between the channel forming sheets.

channels and channels after NTD treatment with 3% P doping. As can be seen from Figure 2, the channels from pristine silicene have a very low capacity until the channel gap reaches 0.75 nm. The strongly corrugated shape of the walls of the nonirradiated channel is significantly deformed during the intercalation of the channel with lithium, which prevents its filling. The situation is corrected only when the channel gap reaches 0.75 nm. Interestingly, as the gap size of the silicene channel subjected to NTD is increased, the channel occupancy by lithium does not increase. Obviously, large values of the gap $h_g$ contribute to an earlier exit of Li atoms from the channel. This is due to the fact that as a result of doping with phosphorus, the walls of the silicene channel become smoother and less susceptible to deformation caused by Li atoms hitting them.

The dependence of the channel filling with lithium on the degree of doping of the silicene walls of the channel with phosphorus is shown in Table 1. It can be seen that the

**Table 1. Maximum Number of Lithium Atoms Obtained as a Result of Intercalation in P-Doped ($N_{Li\ (NTD)}$) Silicene Channels Depending on the Degree of Doping**

| | $N_P$ (%) | | | | |
|---|---|---|---|---|---|
| $N$ | 0 | 3 | 6 | 9 | 18 |
| $N_{Li(NTD)}$ | 12 | 244 | 271 | 72 | 72 |

maximum channel capacity is achieved when its walls have 6% P doping. Also, a high degree of channel occupancy is achieved with 3% doping of its walls. In all other cases, the channel capacity with respect to lithium filling is low, especially in the case of an undoped channel. The low channel occupancy at 9 and 18% doping is due to the appearance of sufficiently large holes in the channel walls after the P atoms left their originally occupied places in the tri- and hexavacancies. Our further studies were devoted to establishing the distributions of P and Li atoms, the diffusion of Li in the channels, and the calculation of the stresses in the walls of the channels filled with lithium. These studies were performed for channels with a gap of 0.24 nm, and their results are shown in Figures 3−11.

Phosphorous atoms are shifted inward to the channel and are located along the boundaries of the corresponding vacancy defects (Figure 3). Transmission electron microscopy analysis

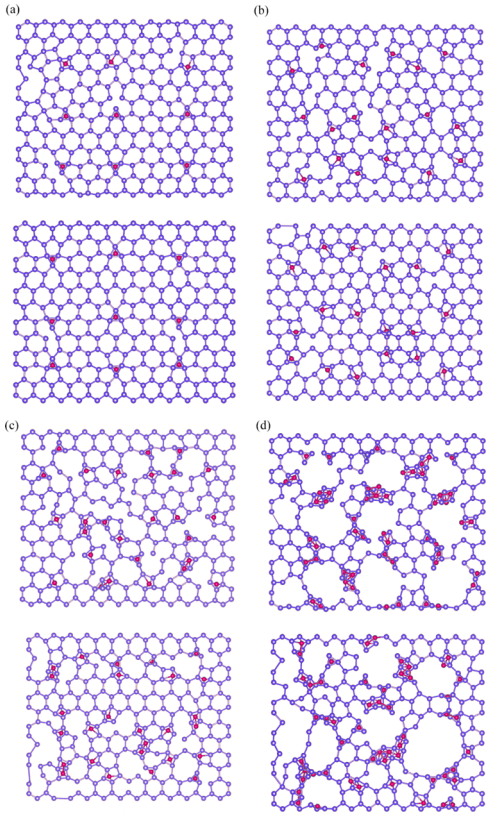


**Figure 3.** Xy-projections of silicene sheets (upper field—upper sheet, lower field—lower sheet) for various degrees of doping: (a) 3, (b) 6, (c) 9, and (d) 18%.



https://dx.doi.org/10.1021/acsomega.0c01240
ACS Omega 2020, 5, 13207−13218

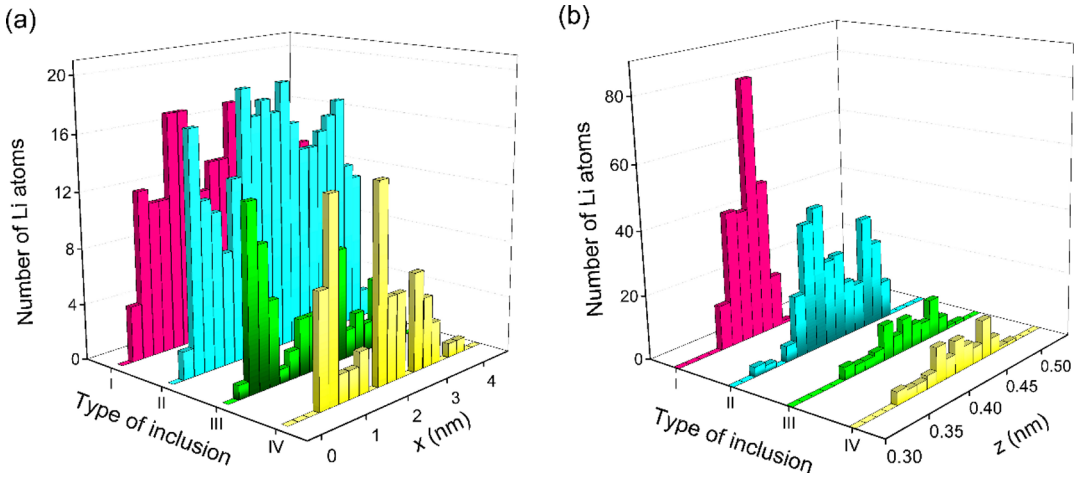


**Figure 4.** Lithium density profiles: (a) along the 0*x* axis and (b) along the 0*z* axis in the channel, which are obtained as a result of intercalation of Li ions into the channel with NTD-treated silicene walls; P atoms fill: I, II, II, and IV—mono-, bi-, tri-, and hexavacancies in silicene, respectively.

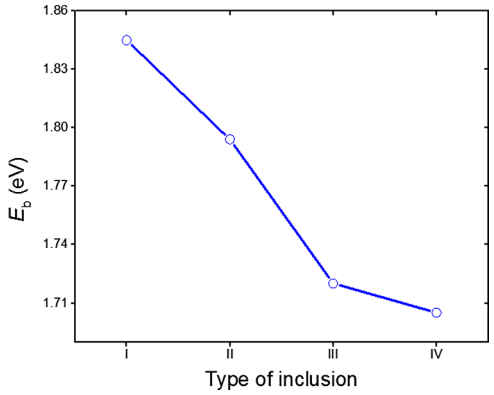


**Figure 5.** Binding energy $E_b$ of Li atoms with doped silicene as a function of phosphorous dopant.

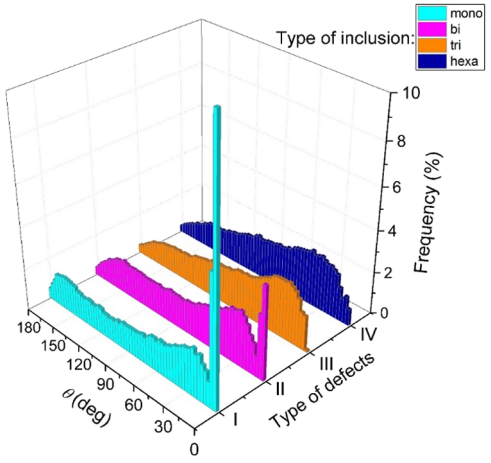


**Figure 7.** Angular distributions of the nearest geometric neighbors for lithium packings obtained in the final stage of intercalation into the channels of modified silicene with defects (I—mono-, II—bi-, III—tri-, and IV—hexavacancies) originally filled with phosphorus atoms.

of an ultrathin P−$SiO_2$ film showed that P atoms are concentrated in a Si-rich region. They are embedded in Si nanocrystals (NCs) formed during high-temperature heat treatment.[27] It can be seen that the form of tri- and hexavacancies is better preserved in the upper sheets of silicene than in the lower sheets, although this difference is

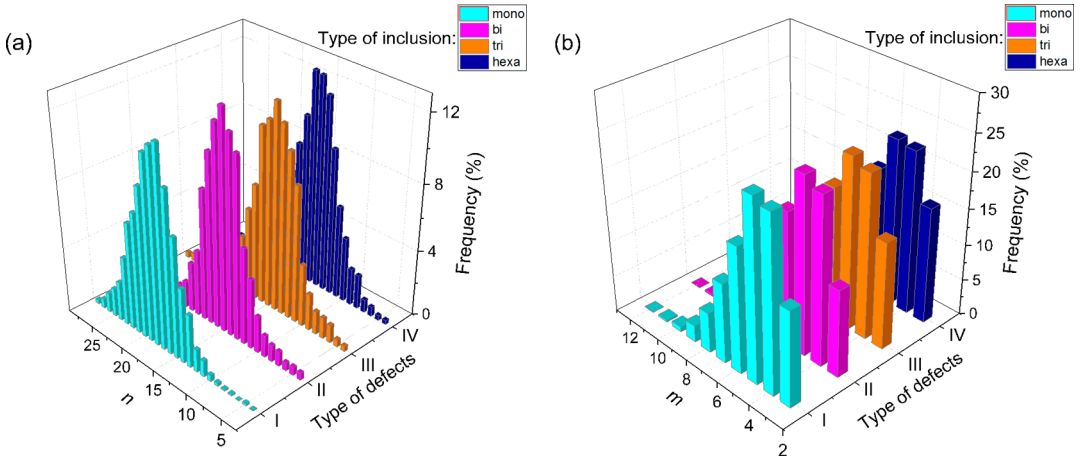


**Figure 6.** (a) Distribution of polyhedra according to the number of faces obtained at the final stage of intercalation of lithium into the channel upon initial filling with P atoms of mono-, bi-, tri-, and hexavacancies; (b) distribution of the faces of the VP according to the number of sides for the packing of lithium in the channels; the spectra presented correspond to the states of the system shown in Figure 4a.



https://dx.doi.org/10.1021/acsomega.0c01240
*ACS Omega* 2020, 5, 13207−13218

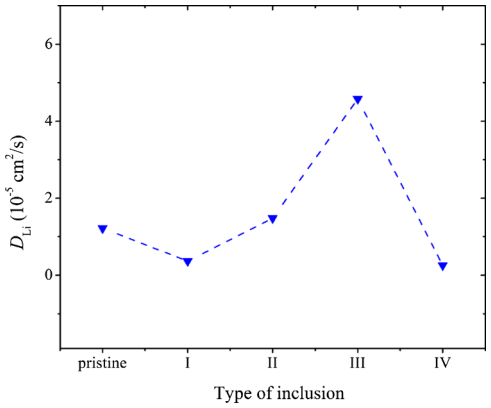


**Figure 8.** Diffusion coefficient of Li atoms during intercalation in the pristine silicene channel and in the Si channel with P atoms initially filling: I, II, II, and IV—mono-, bi-, tri-, and hexavacancies in silicene, respectively.

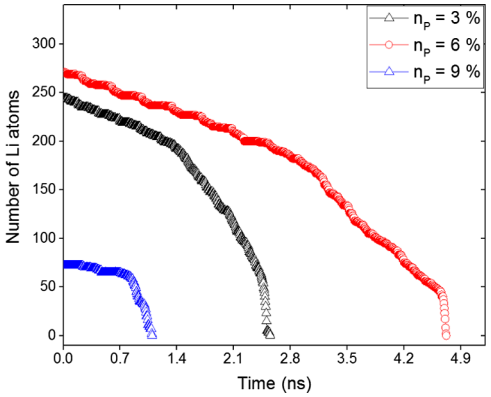


**Figure 9.** Decrease in the number of lithium atoms during deintercalation in a silicene channel with a different degree of doping.

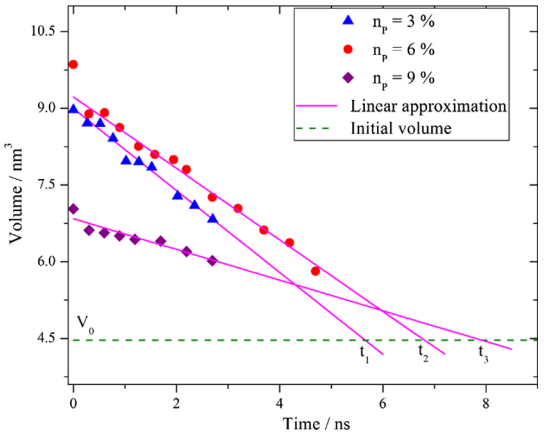


**Figure 10.** Change in the volume of a silicene channel with a different degree of doping (np) during deintercalation; $t_1$, $t_2$, and $t_3$ are the times of reaching the initial volume $V_0$ at 3, 6, and 9% doping of the channel walls, respectively.

erased in the presence of bi- and monovacancies in the sheets of silicene. The latter, as a rule, disappear with the formation of adjacent five- and three-link rings. P atoms are often bonded to three and four Si atoms.

The distribution of Li atoms along the length and height of the modified silicene flat channel obtained at the final stage of intercalation at 3, 6, 9, and 18% doping of silicene with phosphorus is shown in Figure 4. As can be seen from the figure, the channel is filled most densely and uniformly in the direction of the electric field strength vector (directed along the channel length) with lithium at 3 and 6% doping of silicene with phosphorus. With 9 and 18% doping, this filling becomes extremely uneven. In both cases, quite a lot of Li atoms are concentrated near the entrance to the channel, thereby complicating the further movement of $Li^+$ ions deeper into the channel. In this case, the filling of the channel with lithium drops sharply. For a channel with 3% doping of silicene with phosphorus, dense filling of the inner space in the middle of its height is observed. The broadening of this distribution occurs due to giving the paired sheets of silicene a convex shape as a result of the dense filling of the channel with lithium. At 6% doping, the channel continues to be well filled with lithium, and the density distribution over the channel height becomes wider because of the penetration of Li atoms into the opening bivacancies. The opening of vacancy defects is associated with the movement of P atoms filling them into the channel. With a further increase in the size of vacancy defects, which causes a decrease in the filling of the channel with lithium, there occurs a strong displacement of P atoms inside the channel and filling of the formed vacancies with Li atoms. The distribution of the numerical density over the channel height in these cases has a low intensity and extends to a wide range of heights.

Figure 5 shows the binding energy ($E_b$) of intercalated into the doped silicene channel Li atoms.

The binding energy, calculated by us for the lithium atom with the channel walls with different degrees of doping lies in the range $1.70 \leq E_b \leq 1.85$ eV. The binding energy calculated for the most favorable adsorption sites for the Li atom on silicene is ~2.1 eV.[28] As the P concentration increases, from 3 to 6%, the $E_b$ was decreased by 3%, with a further increase in phosphorus concentration , decrease in the binding energy is continuing and reaches a minimum at a phosphorus concentration of 18%. Most likely, in the first systems (3 and 6% P-doped systems), Li atoms occupies energetically more favorable places near the channel walls. However, in the case when the degree of doping is 9 or 18%, the relief of the channel walls changes significantly because of the displacement of a significant number of P atoms inside the channel. At the same time, the number of favorable sites for the adsorption of lithium atoms decreased. Therefore, Li uniform distribution along the walls becomes impossible.

The distribution of Voronoi polyhedra (VP) over the number of faces at the final stage of channel intercalation with lithium shows that the distribution maximum location shifts from $n = 16$ to $n = 14$ when the type of defects initially filled by P atoms changes from mono- to hexavacancies, respectively (Figure 6a). In this case, the standard deviation of the $n$ distribution increased by 13.6%. With an increase in P atoms in the system, the packing of lithium atoms becomes more diverse and more irregular. In all the cases considered here, the distribution maximum location of the faces of the VP by the number of sides falls on $m = 5$ (Figure 6b). This indicates that around each chosen atomic center (the center of the VP), cyclic formations of 5 units are most often formed, which is typical for irregular packing of atoms.[29,30] The standard deviation for the $m$ distribution corresponding to the presence of hexavacancies filled with P atoms increased by only 2.9% relative to the corresponding distribution for the system in which monovacancies are filled with P atoms. Thus, during the


https://dx.doi.org/10.1021/acsomega.0c01240
ACS Omega 2020, 5, 13207−13218

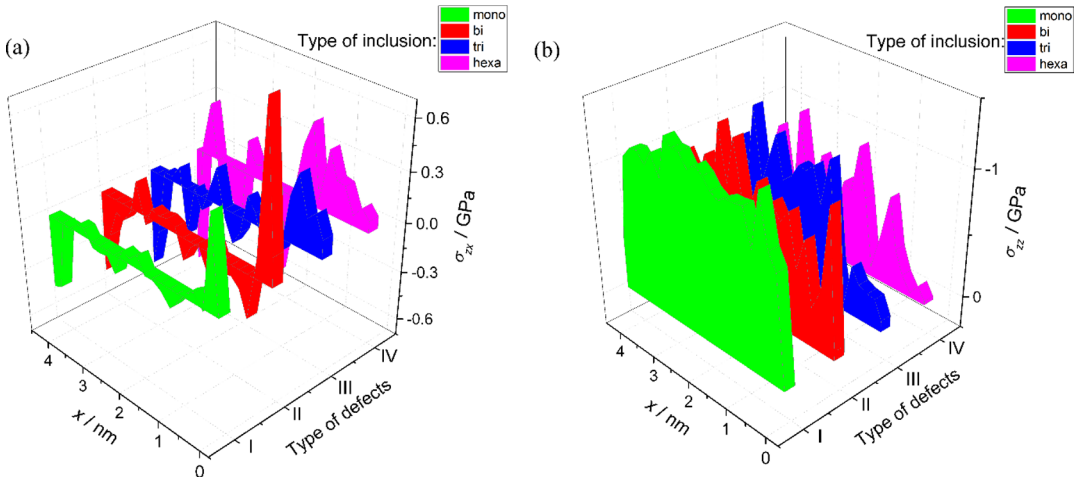


**Figure 11.** $\sigma_{zx}$ (a) and $\sigma_{zz}$ (b) stress tensor component distribution obtained during the intercalation period with lithium in a silicene channel with defects initially filled with P atoms. The channel with a gap of 0.24 nm is located on a graphite substrate, which has a 6.6% doping with nitrogen. The intercalation time is 5.2 ns.

transition from the system I to system IV, the *m* distribution is subject to a smaller change than the *n* distribution.

The angular distributions of the nearest geometric neighbors calculated at the final stage of intercalation in silicene channels with phosphorus doping of 3, 6, 9, and 18% are shown in Figure 7. A feature of these distributions is the presence of sharp peaks at 0° in the case of 3 and 6% doping with phosphorus and the complete absence of such peaks with heavier doping. This means that in lithium packages obtained in the channels of the last two types, there are practically no cases when the Li atoms are on the same line passing through the center of the polyhedron (the center of the Li atom for which VP is built). Distributions of this type cannot be either a completely irregular structure or an ordered (crystalline) structure.[31] The presence of sharp peaks, to some extent, reflects the regularity of packing of Li atoms. Significantly greater with P atoms.

The diffusion coefficient *D* of lithium atoms was calculated through the mean-square displacement of these atoms.[20] The values of the diffusion coefficient *D* of Li atoms in the channel turn out to be weakly correlated with the channel occupancy by lithium (Figure 8). Li atoms in channels from pristine silicene and silicene with mono- or bivacancies have fairly close *D* values. The P atoms that separate from the channel walls begin to strongly influence the diffusion of lithium in the channel when the doping reaches 9%, that is, in the case of the initial filling by P atoms of trivacancies. At the same time, a large rarefaction of the channel contributes to an increase in *D*. However, at 18% doping, when hexavacancies were initially filled with P atoms, the value of *D* drops sharply because of the presence of a large number of P atoms inside the channel that interfere with the diffusion of Li atoms.

The time dependences of the number of Li atoms remaining in the channel during deintercalation are shown in Figure 9. As can be seen from the figure, the channel is completely released from lithium atoms when the silicene walls of the channel have 3% doping with phosphorus, and with 6% doping, the time of the channel being completely released from lithium is the greatest. This is due to the fact that the local surface curvature of the modified silicene obtained as a result of lithium intercalation, enhanced by the displacement of P atoms, is greatest at 6% doping. The local surface curvature, in this case, is even 30% higher than the corresponding value for undoped silicene. As expected, with a decrease in the number of Li atoms in the channel, the time of their exit from the channel also decreases. This is especially noticeable at the final stage of deintercalation with a very low degree of channel filling with lithium. During deintercalation, a channel with 18% of phosphorus-doped walls is destroyed. Therefore, deintercalation in this channel is not shown in Figure 9. One of the reasons for the destruction of this channel is a significant shift of a large number of P atoms from hexavacancies to the channel. During deintercalation, lithium ions involve Li atoms in motion. The P atoms, which impede this movement, pull Si atoms along with them. In addition, with such large defects located over a small area, some Si−Si bonds are very weak. All these circumstances are the cause of the destruction of heavily (18%) phosphorus-doped silicene.

Let us consider the time dependence during deintercalation of the volume of space available for Li atoms in the channel (or channel volume). In none of the studied cases of deintercalation, did the channel volume return to its initial value $V_0$. For the case of fast deintercalation (with 3% doping of the walls of the silicene channel with phosphorus), we extended the calculation from 1.1 ns to $t$ = 2.7 ns in order to confirm the linear nature of volume recovery in the absence of Li atoms inside the channel. We will approximate this dependence $V(t)$, as well as similar dependencies for the cases of 6 and 9% doping, with linear dependences (Figure 10). The intersection of the approximation lines with the horizontal dashed line representing the initial channel volume $V_0$ gives the channel volume recovery times $t_1$ = 5.65 ns, $t_2$ = 6.79 ns, and $t_3$ = 7.90 ns at 3, 6, and 9% doping, respectively. The reliability of the linear approximation was calculated by the formula

$$R^2 = 1 - \left(\frac{\sigma^2}{\sigma_y^2}\right) \quad (2)$$

where $R^2$ is the determining criterion, $\sigma^2$ is the variance of a random variable, and $\sigma_y^2$ is the variance of the dependent variable (volume defined in the model used). The approximation is considered accurate if the condition is fulfilled: $R^2 \approx$



https://dx.doi.org/10.1021/acsomega.0c01240
ACS Omega 2020, 5, 13207−13218

1. The reliability of the linear approximation for these systems is $R^2$ = 0.98, 0.72, and 0.83 at 3, 6, and 9% doping, respectively.

The stress tensor $\sigma_{\gamma\alpha}$ calculated according to formula 4 reflects the nature of the average elastic stresses appearing in the channel walls. The stress tensor was calculated throughout the entire intercalation period. The stresses averaged over both silicene sheets from the forces acting in the *xy* plane and perpendicular to this plane are shown in Figure 11. The stresses shown in the figure are determined in the region of elastic strains arising from the intercalation of lithium into silicene channels. The vector of electric field strength, having a value of $10^4$ V/m, is directed along the axis 0*x* (zigzag direction). The stresses $\sigma_{zx}$ (Figure 11a), caused by forces acting in the plane of the silicene sheet, are most significant at the entrance to the channel for channels with 3 and 6% doping with phosphorus, and for channels with 9 and 18% doping, they are maximum near the exit from the channel. Stresses from the forces of the perpendicular direction $\sigma_{zz}$ are higher than the $\sigma_{zx}$ stress. In the middle part of the sheets, the stresses $\sigma_{zz}$ (Figure 11b) are higher than at their edges, that is, at the entrance and exit of the channel. These stresses are distributed more evenly (than $\sigma_{zx}$ stresses) over the surface of silicene sheets, especially in the case of 3% doping of silicene with phosphorus. However, at 6−18% P-doping, the $\sigma_{zz}$ distribution has an uneven serrated character. The change in the behavior of the stress distribution depending on the degree of doping is due to a change in the nature of the filling of the channel with lithium depending on the size of the vacancy defects initially filled with P. Because of the very thin bridges between the pores formed in silicene with 18% phosphorus doping, the transition from elastic to inelastic deformation during cycling occurs very quickly (less than 1 ps). In this case, the breaking of Si−Si bonds in the bridging region leads to the destruction of the silicene sheet.

Doping of silicene was performed in order to change its electronic and magnetic properties, that is, for the same purposes as is usually done for crystalline silicon.[32] Modulation of magnetism and the corresponding electronic structures appeared due to spin splitting caused by impurity and was carried out for armchair silicene nanoribbons by doping with P or Al.[33] It was shown that the doping result strongly depends on the doping location and the width of the tape. The phosphorus and boron atoms included in silicon NCs upon doping thermodynamically prefer to be on the NC surface.[34] However, upon doping of bulk Si and heavy doping of Si NC, they replace Si atoms. One can expect the separation of B and P on the NC surface.

An estimate of the effective specific energy density for a LIB with an anode that functions as a freestanding bilayer silicene gives a value of ∼2100 W h $kg^{-1}$.[16] This value exceeds by more than an order of magnitude the corresponding characteristic for the LIB currently used.[35] Currently, the anode materials in serial LIBs are typically graphite. Improvements in the electrochemical properties of this material can be achieved by doping with nitrogen. Nitrogen is more electronegative than carbon. In addition, during doping, hybridization occurs between the lone pair of nitrogen electrons and the $\pi$-electrons of the graphene system.[36] For nitrogen-doped graphene nanosheets, a reversible capacity of up to 900 mA h/g can be achieved with high cyclicity.[37] In fact, in the battery design considered here, graphite is not an active material, and the effect of increasing the battery capacity is achieved through the use of silicene.

In the molecular dynamics (MD) model, the functioning of the elementary electrochemical cell, representing the element of a new-generation LIB, is investigated. Silicene on a graphite substrate after their transmutation neutron doping is used as an anode. As a result of doping, phosphorus appears in silicene and nitrogen in graphite. Phosphorus is more electronegative than silicon. The degree of doping with phosphorus is in the range of 3−18%, and the degree of doping with nitrogen is 5%. Doping increases the occupancy rate of lithium channels with gaps from 0.65 to 0.24 nm by 7−20 times and a channel with a gap of 0.75 nm by 1.15 times. The highest lithium filling of the channel with a gap of 0.24 nm is observed at 6 and 3% doping of silicene with phosphorus. The largest filling of the channel with lithium at the smallest gap considered here is mainly due to two reasons. First, as a result of heavy alloying, the channel walls straighten, that is, silicene loses its corrugated shape, becoming almost flat (with the exception of P atoms extending beyond the surface). Such a surface of the channel walls allows $Li^+$ ions to enter the channel and move along it without interference. Second, because of the flexibility of silicene and the flexibility of Si−Si bonds, the lithium-filled channel acquires a convex shape with a narrowing at the inlet and outlet. This channel shape contributes to the retention of lithium atoms in it. With an increase in the size of opening defects (polyvacancies) due to the departure of P atoms from them, there are more and more possibilities for the escape of Li atoms through the resulting pores. As a result, the filling of the channel with lithium is sharply reduced at 9 and 18% doping with the phosphorus of the channel walls.

Our calculations show that P atoms when doping silicene prefer to be on its surface if the phosphorus concentration is from 3 to 18%. The escape of P atoms from substitution sites to the surface is accompanied by a rearrangement of the defective structure of silicene. In the case of the initial single and paired arrangement of P atoms (in monovacancies and bivacancies) after displacement, they, as a rule, form bonds with three Si atoms on the surface of silicene and do not contact each other. However, in the case of the initial proximity of three P atoms (when filling the trivacancy), the bond between two P atoms can remain after they reach the silicene surface. When immediately the defect was initially filled with six P atoms, freeing the hexavacancy, they were placed on the surface of the defective silicene in groups containing from 2 to 7 P atoms. In all the cases considered, very few Li atoms are found near the channel walls, when they are located above the centers of the hexagonal rings formed by Si atoms. In this way, packings of lithium atoms in channels with alloyed walls differ from the corresponding packings in channels formed by sheets of pure silicene and located on metal substrates.[19−21]

At 3 and 6% doping with phosphorus, Li atoms fairly uniformly both along the length of the channel and along with its height filled the silicene channel during intercalation. However, upon the opening of bivacancies (after the departure of P atoms), the space adjacent to them in the upper sheet of silicene was filled with Li atoms. The lithium filling of channels with silicene walls subjected to 9 and 18% doping was hampered by the presence of a large number of P atoms in the channel and the associated channel deformation.

Structural analysis performed by the method of statistical geometry shows that the packing of Li atoms in the channel is largely irregular. This is evidenced, for example, by the distribution of VP faces by the number of sides. For all


https://dx.doi.org/10.1021/acsomega.0c01240
ACS Omega 2020, 5, 13207−13218

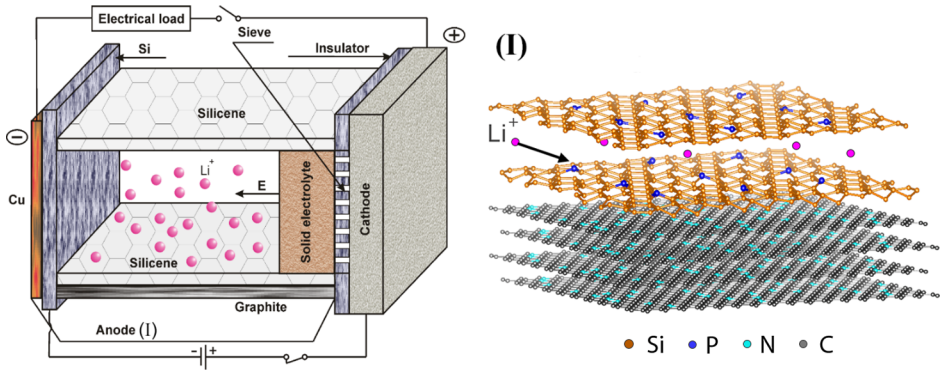


**Figure 12.** Schematic diagram of the cell LIB with a silicene anode; (I) simulated in this study MD system.

channels considered here, the maximum of $m$ distribution falls on $m = 5$, that is, fifth-order rotational symmetry, which is not characteristic of crystals, prevails in the packing of Li atoms. Such symmetry is usually manifested in irregular packings for liquids and amorphous bodies.[38,39] However, the presence of flat walls makes its own adjustments to the nature of the packing of lithium atoms. In particular, the spectra of the angles of the mutual arrangement of the nearest geometric neighbors have a shape that is very different from that for both liquid and crystal. This is especially true for the $\theta$ distribution obtained in the silicene channel, the walls of which had 3% doping with phosphorus. In this case, the presence of P atoms in the channel had a minimal effect on the formation of the packing of Li atoms.

The diffusion coefficient of lithium ions in the new-generation LIB should be of the order of $10^{-5}$ $cm^2/s$. The high value of the coefficient $D$ makes it possible to obtain a high rate of charging LIB. In the region of silicene doping with phosphorus considered here, the values of $D$ required for the development of LIB are achieved. However, because of the high density achieved by intercalating lithium into the channel, the coefficient $D$ can decrease, as is the case with 3% doping of silicene with phosphorus.

When the battery is discharged, a gradual decrease in operating voltage is observed. However, the natural process of deintercalation takes too much time. It is difficult to trace directly with MD modeling. For analyzing this process, an artificial technique was used in the present work, the essence of which was to study deintercalation by applying a constant electric field in the opposite direction. The more completely the silicene channel was filled with lithium during intercalation, the more time was required for the channel to be completely released from lithium. An extrapolation-statistical estimation of the recovery time of the channel volume, determined from the start of deintercalation to achievement of initial volume value, showed that this time increases with the size of defects, that is, polyvacancies that were initially filled with P atoms. The estimated values of the channel volume recovery time ranged from 5.65 to 7.90 ns, which is 11−16 times longer than the time used to fill the channel with lithium in the present work.

Knowledge of the mechanical properties of silicene provides useful information for its use in various devices based on nanoelectronics as well as in electrochemical cells. Silicene has a tensile strength of ∼12.5−19.5 GPa and a maximum strain of about 18%.[13,40] In tensile tests, silicene behaves differently than graphene. It is split both along the zigzag edge and along the edge of the armchair, while graphene is torn only along its zigzag edge.[41] Our calculations show that in all considered cases of intercalation, the anodic material of doped silicene has more than a ten-fold safety factor with respect to the ultimate tensile stress.

## CONCLUSIONS

The design of a solid electrolyte LIB cell is proposed, which allows the creation of batteries with a high energy density and fast charging, environmental, and explosion proof. The MD method demonstrated the functioning of such an element during intercalation and deintercalation of lithium. The active element of the battery anode is a two-layer silicene on a graphite substrate, previously subjected to a controlled procedure of heavy alloying. Doping leads to straightening of the profile of the silicene sheet because of which the penetration of lithium ions into the planar silicene channel is greatly facilitated. In the presence of mono- and bivacancies filled with phosphorus atoms in the silicene walls of the channel, the complete filling of the channel with lithium was observed at the initial gap, which is natural for two-layer silicene. The capacity of the anode drops sharply when the size of defects in silicene increases, which is already observed in the presence of tri- and hexavacancies. In all cases, phosphorus atoms, which initially fill vacancy defects, enter the surface of silicene sheets and, in the absence of adjacent P atoms, bind to three Si atoms. At high phosphorus concentrations, the P−P bonds are also formed on the surface of silicene sheets. Lithium atoms in such channels form mostly irregular packing. A pronounced effect of the channel walls on the packing of lithium atoms in it is observed only in the presence of mono- and bivacancies that open after the P atoms enter the surface. High diffusion coefficients of lithium atoms should lead to the fast charging of the battery. Slowing down the diffusion of lithium atoms when filling the channel can occur in the presence of mono- and hexavacancies in the silicene walls. After the channel is completely released from lithium, a certain time is required to restore its original volume. The stresses normal to the walls of the channel filled with lithium are higher than the longitudinal stresses. The uniform distribution of normal stresses is replaced by a substantially inhomogeneous distribution with an increase in the size of defects in the channel walls. The intercalation of lithium in silicene channels does not lead to stresses that can destroy its walls.

Thus, the proposed design of the LIB cell with an appropriate selection of structural materials can be used to create miniature, environmental, safe batteries with high capacity, energy density, and fast charging.


https://dx.doi.org/10.1021/acsomega.0c01240
ACS Omega 2020, 5, 13207−13218

## COMPUTATIONAL METHODS

In the present study, the composite anode lithization and delithization processes were modeled by using the MD method. The schematic diagram of the electrochemical cell under consideration is shown in Figure 12. The electric field direction, the silicene, and graphite sheet location are also demonstrated in Figure 12. The system investigated in this work is highlighted on the general view of LIBs as (I) and presented on the inset (I).

It is assumed that the silicene and graphite shown in the figure can be subjected to transmutation neutron doping. The LIB cell is fully solid-state. The anode part of the element consists of a copper current collector, a silicon film deposited on it, and perpendicular to it sheets of silicene, one of which is on a graphite substrate. Both sheets of silicene are bonded to a nanostructured silicon film by electrical discharge. Between the sheets of silicene is a solid electrolyte, which through a molecular sieve is in contact with the cathode. Between the sheets of silicene, including a sheet located on a graphite substrate, and the cathode, an insulating film is located, at the point of contact of which with the electrolyte, a molecular sieve is created. The sieve allows lithium ions to pass from the solid electrolyte to the cathode and vice versa. When the cell is charged, $Li^+$ ions under the influence of a constant electric field exit the electrolyte and rush mainly toward the film of nanostructured silicene. Because of the movement along the lines of the electric field directed toward the silicene sheets, as well as in collisions, they lose energy and are deposited on the surface of silicene, and at high density, they also fill the central part of the silicene channel. Some ions are deposited on a nanostructured silicon surface. Such a movement makes it possible to fill the silicene channel with $Li^+$ ions as densely as possible. When the battery is discharged, the lithium ions move in the opposite direction.

Sheets of silicene having a floral structure[42] were arranged horizontally, one above the other. The unit cell of silicene had a rhombic shape and contained 18 atoms, 6 of which were elevated relative to the basal plane.[43] The sheets of silicene were oriented with respect to each other so that the protrusions on their surface were facing outward. The silicene channel in the computer model was represented by a bilayer silicene, whose gap between the sheets could vary in the range from 0.24 to 0.75 nm. The value $h_g$ = 0.24 nm was determined in DFT calculations as a gap in a two-layer freestanding silicone.[44] The size of the silicene sheet was 4.1 × 4.8 nm, and in the case of pristine silicene, a sheet consisted of 300 Si atoms. The channel was located on a graphite substrate completely overlapping a silicene sheet, consisting of four parallel graphene sheets stacked according to Bernal packaging {ABAB ...}. The entire graphite substrate was represented by 2720 C atoms. The distance between the lower silicene sheet and the upper carbon substrate sheet was 0.222 nm and exactly corresponded to such a distance determined in the DFT calculation.[45] In this work, in contrast to refs,[19−21] no artificial barrier was created along the sides and rear of the channel to prevent the escape of Li atoms. Not all ions that started moving toward the channel entered into it and remained there during the whole time of the computer experiment. Some of the lithium ions (atoms) overcame the potential binding with the silicon atoms and left the channel. In the case when doped silicene was used as channel walls, it was possible for lithium atoms to exit the channel through the holes formed at the sites of substitution of Si atoms by P atoms.

The intercalation of lithium was performed by sequentially introducing $Li^+$ ions through the front surface of the channel. A band identical to the channel entrance section was moved along the 0$x$ axis outward (to the left) from the channel entrance by a distance of 0.5 nm. Random points within this band served as the initial locations of $Li^+$ ions. Ions were introduced one at a time at regular intervals, the duration of which was 1 ps. The initial direction of ion motion coincided with the 0$x$ axis (zigzag direction in silicene), along which a constant electric field with a strength of $10^4$ V/m acted. Such an electric field strength can be achieved in an electrolyte, which is enclosed between the $LiC_6$ cathode and the $LiCoO_2$ anode of the thin-film LIB. The distance between the cathode and anode was 28 $\mu$m.[46] The ions gradually entering the channel retained their electric charge for 1 ps. Each emitted ion turned into a neutral Li atom at the moment of launching of the next ion. Thus, the lifetime of each ion was limited to 1 ps. When choosing the ion lifetime in the channel, we were guided by the following fact. According to the classical concept of terahertz radiation, the achievable pulse duration of a short electron beam is ∼1 ps.[47] We take this value for the time of spontaneous emission of an electron. At the same time, recombination of the $Li^+$ ion in the silicene channel should occur. It has been experimentally established that $Li^+$ ions falling into silicon combine with electrons to form lithium atoms.[48] This is facilitated by the fact that the $Li_xSi$ compounds formed in silicon have a higher electronic conductivity than silicon. Unlike graphite, Li atoms diffuse in the volume of silicon, but ions do not.[49] The time step for integrating the equations of motion was 0.1 fs. Previously, all studied systems were balanced within 100 ps or 1 million time steps. Then, the channel was filled with lithium for 500 ps.

The deintercalation of lithium from the channel was carried out by changing the direction of the vector of the electric field strength in the opposite direction with respect to its direction during intercalation. Lithium atoms sequentially acquired a charge and became $Li^+$ ions, and the sequence of their exit from the channel was changed to the opposite sequence of their entrance to the channel. Thus, the last ion entering the channel exited from it first. It was previously shown that the order of ion exit from the channel does not fundamentally change the nature of the deintercalation process.[21] The magnitude of the electric field during deintercalation remained the same ($10^4$ V/m). However, in order to achieve the complete release of the channel from $Li^+$ ions, the deintercalation time had to be increased. This is especially true of deintercalation in a channel with 6% doping of silicene walls with phosphorus, where the time of the reverse process increased by almost an order of magnitude.

Modeling of silicene doping was carried out by creating vacancy defects in its sheets and filling them with phosphorus atoms. Moreover, the P atoms occupied the same locations as the excluded Si atoms. On each sheet of silicene, nine vacancy defects were formed, which were approximately uniformly distributed over the surface of the sheet. These defects were mono-, bi-, tri-, and hexavacancies. Therefore, the phosphorus content in the sheets of silicene was 3, 6, 9, and 18%. When silicon is irradiated with thermal neutrons, some Si atoms are transmuted into phosphorus atoms, and silicon acquires n-type impurity conductivity. The carbon substrate subjected to the NTD procedure in all cases considered here had a rather heavy


https://dx.doi.org/10.1021/acsomega.0c01240
ACS Omega 2020, 5, 13207−13218

5% doping with nitrogen. Heavily nitrogen-doped graphite NG (up to 10.17%) is a catalyst for the reduction of nitroarenes in water with a small amount of $NaBH_4$.[50] In the literature,[50] NG was produced from graphene oxide with nitrogen concentrations of 4.23, 6.33, 7.16, and 10.17%. In the present work, 6.6% doping of a graphite substrate with nitrogen was carried out. This level of doping exceeds the light isotope-oriented level of doping of graphite. The natural abundance of $^{13}C$ carbon, from which the unstable $^{14}C$ isotope is formed as a result of neutron transmutation, is 1.1%. An increase in the time of exposure to thermal neutrons makes it possible to increase the degree of doping.

The interactions ($Si^{(k)}$–$Si^{(k)}$) between Si atoms of the same $k$-sheet of silicene, as well as the interactions $C^{(l)}$–$C^{(l)}$ between C atoms belonging to the same graphite $l$-layer, were described by Tersoff's many-particle potential.[51,52] The remaining interactions were presented in the form of the Morse potential[53]

$$\Phi(r) = D_e[\exp\{-2\alpha(r - r_e)\} - 2\exp\{-\alpha(r - r_e)\}] \quad (3)$$

where $r$ is the pair interatomic distance and $D_e$, $\alpha$, and $r_0$ are the fitting parameters. The parameters of the Morse potentials used here are presented in Table 2.

**Table 2. Morse Fitting Parameters for the Pair Interatomic Interactions[a,b]**

| interaction | $D_e$, eV | $\alpha$, Å$^{-1}$ | $R_e$, Å |
|---|---|---|---|
| N–N | 2.275 | 2.233 | 1.342 |
| N–Si | 0.21326 | 3.813 | 2.4572 |
| N–C | 4.440 | 2.096 | 1.350 |
| N–P | 1.66665 | 2.2775 | 2.03591 |
| P–P | 1.001 | 2.322 | 2.263 |
| P–Si | 4.479 | 2.301 | 1.300 |
| P–C | 1.55737 | 2.4385 | 2.38899 |
| $Si^{(i)}$–$Si^{(j)}$ | 0.2274 | 1.539 | 4.4992 |
| $C^{(i)}$–$C^{(j)}$ | 2.4230 | 2.5550 | 2.522 |
| Si–C | 0.435 | 4.6487 | 1.9475 |
| Li–Li | 0.42076 | 0.7899 | 3.000 |
| Li–Si | 0.309323 | 1.16445 | 3.67390 |
| Li–C | 1.258510 | 1.70745 | 2.06470 |
| Li–P | 0.64898 | 1.55595 | 2.60557 |
| Li–N | 1.08055 | 1.51145 | 2.00648 |

[a]Cutoff distance is 2.0 Å for C–C and C–N interactions and 3.0 Å for Si–P and P–P interactions. [b]The superscripts $i$ and $j$ indicate different sheets of silicene or graphene.

The emergence of a lithium atom from the $Li^+$ ion occurred through a time interval of 1 ps. This time determines the lifetime of a lithium ion. The difference in the description of the interactions of $Li^+$ and Li with the environment was that the lithium ion was sensitive to the applied electric field, but the lithium atom was not. In other words, the $Li^+$ ion having an electric charge +1$e$, during its lifetime, besides the usual atomic (without changing the shape of the potentials and their parameters) interaction with the environment, had a Coulomb interaction with an applied electric field. Thus, while the ion existed, the force of the electric field, pushing the ion to move in the direction of the field strength, was added (as a vector) to the force acting on ion from the surrounding environment. Such an additional force did not participate in the dynamics of the electrically neutral atom of Li.

The effect of lithium introduced into the channel on silicene leads to the appearance of stresses that propagate along the channel walls. To establish stress distribution, we divide the sheets of silicene into elementary areas with the normal $\gamma$ ($x$, $y$, $z$) and elongated either in the "armchair" direction or in the "zigzag" direction. Next, the resulting force acting on each of the areas is determined. In determining the resultant force, only those interactions between particles $i$ and $j$ are taken into account, the force vector of which pierces the given area.[20] Then for the $\sigma_{\gamma\alpha}(l)$ stress acting on the $l$-area, we can write

$$\sigma_{\gamma\alpha}(l) = \left\langle \sum_i^n \frac{1}{\Omega}(m v_\gamma^i v_\alpha^i) \right\rangle + \frac{1}{S_l}\left\langle \sum_i^n \sum_{j\neq i}^{(u_i\le u, u_j\ge u)} (f_{ij}^\alpha) \right\rangle \quad (4)$$

In expression 4, the following notation is used: $n$ is the number of atoms on the $l$th area, $\Omega$ is the volume per atom, $m$ is the atomic mass, $v_\alpha^i$ is the $\alpha$ projection of the velocity of the $i$th atom, $S_i$ is the area of the $l$th surface element, $f_{ij}^\alpha$ is the $\alpha$ projection of the force resulting from the interaction of $i$ and $j$ atoms and passes though the $l$th area, and $u_i$ is the coordinate of the atom $i$; the symbol $u$ denotes the coordinate of the contact point of the straight line through the centers of the atoms $i$ and $j$ and the $l$th surface element.

It is very important to determine how strongly lithium atoms intercalated into the channel bind to the channel walls. Substitution of certain atoms in silicene with phosphorus atoms can lead to a change in the adsorption energy of lithium atoms on the channel walls. In turn, this change will affect the channel occupancy. The binding (adsorption) energy per 1 lithium atom was calculated according to

$$E_b = E_0 + xE_{Li} - E_x \quad (5)$$

where $E_0$ is the total energy of two-layer silicene free of intercalated Li atoms, $x$ is the number of Li atoms adsorbed on silicene, $E_{Li}$ is the energy of the isolated Li atom, and $E_x$ is the total energy of the lithiated structure. The energies $E_0$ and $E_x$ are determined in the presence of a graphite substrate and with appropriate doping of silicene and graphite with phosphorus and nitrogen, respectively.

Analysis of lithium packings during intercalation into channels with defects in the form of mono-, bi-, tri-, and hexavacancies, initially filled with phosphorus atoms, can be done using the method of statistical geometry. This method is based on the construction of VP and subsequent statistical analysis of the structural elements of these polyhedra. The most informative among the obtained statistical distributions is the angular distribution of the nearest geometric neighbors, which considers the angles $\theta$ formed by the rays drawn from the center VP to the centers of different pairs of geometric neighbors, that is, neighbors from which the faces of this polyhedron are obtained.[54] Angular distributions $\theta$ began to be calculated after the first 100 Li atoms were intercalated into the channel. Each subsequent configuration with a newly appeared atom (rather than an ion) Li was included in the calculation of the $\theta$ distribution. The number of configurations added in this way corresponded to the number $N_{Li(NTD)}$ −100, where $N_{Li(NTD)}$ is the limiting number of Li atoms intercalated into the channel.

In the present work, the standard LAMMPS code[55] for performing MD modeling was supplemented with fragments that made it possible to calculate the kinetic and mechanical properties of the system. The calculations were performed on a


https://dx.doi.org/10.1021/acsomega.0c01240
ACS Omega 2020, 5, 13207−13218

URAN cluster-type hybrid computer at the IMM UB RAS with a peak performance of 216 Tflop/s and 1864 CPU.

## ■ ASSOCIATED CONTENT

### Supporting Information

The Supporting Information is available free of charge at https://pubs.acs.org/doi/10.1021/acsomega.0c01240.

Dynamics of lithium ions filling a silicene channel located on a graphite substrate (MPG)

## ■ AUTHOR INFORMATION


### Corresponding Author

**Alexander Y. Galashev** − *Institute of High-Temperature Electrochemistry of the Ural Branch of the Russian Academy of Sciences, Yekateirnburg 620990, Russia; Ural Federal University Named after the First President of Russia B.N. Yeltsin, Yekaterinburg 620002, Russia*; Email: galashev@ihte.uran.ru

### Authors

**Ksenia A. Ivanichkina** − *Institute of High-Temperature Electrochemistry of the Ural Branch of the Russian Academy of Sciences, Yekateirnburg 620990, Russia*; orcid.org/0000-0001-6521-1966

**Konstantin P. Katin** − *National Research Nuclear University "MEPhI", Moscow 115409, Russia; Research Institute for the Development of Scientific and Educational Potential of Youth, Moscow 119620, Russia*; orcid.org/0000-0003-0225-5712

**Mikhail M. Maslov** − *National Research Nuclear University "MEPhI", Moscow 115409, Russia; Research Institute for the Development of Scientific and Educational Potential of Youth, Moscow 119620, Russia*; orcid.org/0000-0001-8498-4817

Complete contact information is available at: https://pubs.acs.org/10.1021/acsomega.0c01240


### Notes

The authors declare no competing financial interest.

## ■ ACKNOWLEDGMENTS

This work was performed as part of the agreement no. 075-03-2020-582/1 dated 02.18.2020 (topic number 0836-2020-0037).

## ■ REFERENCES


(1) Gong, B.; Song, X.; Shi, Y.; Liu, J.; Hao, C. Understanding the inhibition of the shuttle effect of sulfides (S ≤ 3) in lithium−sulfur batteries by heteroatom-doped graphene: First-principles study. *J. Phys. Chem. C* **2020**, *124*, 3644−3649.

(2) Haseeb, H. H.; Li, Y.; Ayub, S.; Fang, Q.; Yu, L.; Xu, K.; Ma, F. Defective phosphorene as a promising anchoring material for lithium−sulfur batteries. *J. Phys. Chem. C* **2020**, *124*, 2739−2746.

(3) Pearce, P. E.; Assat, G.; Iadecola, A.; Fauth, F.; Dedryvère, R.; Abakumov, A.; Rousse, G.; Tarascon, J.-M. Anionic and cationic redox processes in β-Li2IrO3 and their structural implications on electrochemical cycling in a Li-ion cell. *J. Phys. Chem. C* **2020**, *124*, 2771−2781.

(4) Galashev, A. E.; Zaikov, Y. P.; Vladykin, R. G. Effect of electric field on lithium ion in silicene channel. Computer experiment. *Russ. J. Electrochem.* **2016**, *52*, 966−974.

(5) Zhou, X.; Yin, Y.-X.; Wan, L.-J.; Guo, Y.-G. Self-Assembled Nanocomposite of Silicon Nanoparticles Encapsulated in Graphene through Electrostatic Attraction for Lithium-Ion Batteries. *Adv. Energy Mater.* **2012**, *2*, 1086−1090.

(6) Zhuang, J.; Xu, X.; Peleckis, G.; Hao, W.; Dou, S. X. Silicene: A Promising Anode for Lithium-Ion Batteries. *Adv. Mater.* **2017**, *29*, 1606716.

(7) Grazianetti, C.; Molle, A. *Engineering Epitaxial Silicene on Functional Substrates for Nanotechnology*; Research, 2019, Article ID 8494606.

(8) Wu, K.-H. A review of the growth and structures of silicene on Ag (111). *Chin. Phys. B* **2015**, *24*, 086802.

(9) Liu, Y.-P.; Ning, B.-Y.; Gong, L.-C.; Weng, T.-C.; Ning, X.-J. A New model to predict optimum conditions for growth of 2D materials on a substrate. *Nanomaterials* **2019**, *9*, 978.

(10) De Padova, P.; Vogt, P.; Resta, A.; Avila, J.; Razado-Colambo, I.; Quaresima, C.; Ottaviani, C.; Olivieri, B.; Bruhn, T.; Hirahara, T.; Shirai, T.; Hasegawa, S.; Carmen Asensio, M.; Le Lay, G. Evidence of Dirac fermions in multilayer silicene. *Appl. Phys. Lett.* **2013**, *102*, 163106.

(11) Quhe, R.; Yuan, Y.; Zheng, J.; Wang, Y.; Ni, Z.; Shi, J.; Yu, D.; Yang, J.; Lu, J. Does the Dirac cone exist in silicene on metal substrates? *Sci. Rep.* **2014**, *4*, 5476.

(12) Wu, D.; Wang, S.; Zhang, S.; Liu, Y.; Ding, Y.; Yang, B.; Chen, H. Stabilization of two-dimensional penta-silicene for flexible lithium-ion battery anodes via surface chemistry reconfiguration. *Phys. Chem. Chem. Phys.* **2019**, *21*, 1029.

(13) Pei, Q.-X.; Sha, Z.-D.; Zhang, Y.-Y.; Zhang, Y.-W. Effects of temperature and strain rate on the mechanical properties of silicene. *Journal of Applied Physics* **2014**, *115*, 023519.

(14) Yao, M.; Ai, L.; Zhou, Y.; Ma, J.; Chen, M. Structural damage of few-layer silicene in vertical and parallel lithiations. *J. Electrochem. Soc.* **2019**, *166*, A3394−A3400.

(15) Xu, S.; Fan, X.; Liu, J.; Singh, D. J.; Jiang, Q.; Zheng, W. Adsorption of Li on single-layer silicene for anodes of Li-ion batteries. *Phys. Chem. Chem. Phys.* **2018**, *20*, 8887−8896.

(16) Galashev, A. Y.; Ivanichkina, K. A. Silicene anodes for lithium-ion batteries on metal substrates. *J. Electrochem. Soc.* **2020**, *167*, 050510.

(17) Aufray, B.; Kara, A.; Vizzini, S.; Oughaddou, H.; Léandri, C.; Ealet, B.; Le Lay, G. Graphene-like silicon nanoribbons on Ag(110): A possible formation of silicene. *Appl. Phys. Lett.* **2010**, *96*, 183102.

(18) Galashev, A. Y.; Ivanichkina, K. A. Computer study of atomic mechanism of intercalation/deintercalation of Li ions in a silicene anode on an Ag(111) substrate. *J. Electrochem. Soc.* **2018**, *165*, 1788−1796.

(19) Galashev, A. Y.; Ivanichkina, K. A. Computer test of a new silicon anode for lithium-ion batteries. *ChemElectroChem* **2019**, *6*, 1525−1535.

(20) Galashev, A. Y.; Ivanichkina, K. A. Computational investigation of a promising anode material. *Phys. Chem. Chem. Phys.* **2019**, *21*, 12310.

(21) Galashev, A. Y.; Zaikov, Y. P. New Si−Cu and Si−Ni anode materials for lithium ion batteries. *J. Appl. Electrochem.* **2019**, *49*, 1027−1034.

(22) Galashev, A. E.; Ivanichkina, K. A. Numerical simulation of the structure and mechanical properties of silicene layers on graphite during the lithium ion motion. *Phys. Solid State* **2019**, *61*, 233−243.

(23) Galashev, A. E.; Rakhmanova, O. R. Graphene and Graphite Supports for Silicene Stabilization: A Computation Study. *J. Struct. Chem.* **2018**, *59*, 877−883.

(24) Zaminpayma, E.; Nayebi, P. Band gap engineering in silicene: A theoretical study of densityfunctional tight-binding theory. *Phys. E* **2016**, *84*, 555−563.

(25) Zhong, H.-X.; Quhe, R.; Wang, Y.; Shi, J.; Lu, J. Silicene on substrates:A theoretical perspective. *Chin. Phys. B* **2015**, *24*, 087308.

(26) Zeng, Z.; Ma, X.; Chen, J.; Zeng, Y.; Yang, D.; Liu, Y. Effects of heavy phosphorus-doping on mechanical properties of Czochralski silicon. *J. Appl. Phys.* **2010**, *107*, 123503.

(27) Perego, M.; Bonafos, C.; Fanciulli, M. Phosphorus doping of ultra-small siliconnanocrystals. *Nanotechnology* **2010**, *21*, 025602.

(28) Tritsaris, G. A.; Kaxiras, E.; Meng, S.; Wang, E. Adsorption and diffusion of lithium on layered silicon for Li-Ion storage. *Nano Lett.* **2013**, *13*, 2258−2263.
(29) Novruzova, O. A.; Rakhmanova, O. P.; Galashev, A. E. The stability and structure of (N2)j(H2O)i and (Ar)j(H2O)i clusters. *Russ. J. Phys. Chem.* **2007**, *81*, 1825−1828.
(30) Galashev, A. Y.; Ivanichkina, K. A. Numerical simulation of the structure and mechanical propertiesof silicene layers on graphite during the lithium ion motion. *Russ. J. Phys. Chem. A* **2017**, *91*, 233−243.
(31) Galashev, A. Y. Atomistic simulations of methane interactions with an atmospheric moisture. *J. Chem. Phys.* **2013**, *139*, 124303.
(32) Zhang, J.-M.; Song, W.-T.; Xu, K.-W.; Ji, V. The study of the P doped silicene nanoribbons with first-principles. *Comput. Mater. Sci.* **2014**, *95*, 429.
(33) Zhang, X.; Zhang, D.; Xie, F.; Zheng, X. H.; Wang, M. L. First-principles study on the magnetic and electronic properties of Al or P doped armchair silicene nanoribbons. *Phys. Lett. A.* **2017**, *381*, 2097−2102.
(34) Pi, X. J. Doping silicon nanocrystals with boron and phosphorus. *Nanomater* **2012**, *2012*, 912903.
(35) Cerdas, F.; Titscher, P.; Bognar, N.; Schmuch, R.; Winter, M.; Kwade, A.; Herrmann, C. Exploring the effect of increased energy density on the environmental impacts of traction batteries: A comparison of energy optimized lithium-ion and lithium-sulfur batteries for mobility applications. *Energies* **2018**, *11*, 150.
(36) Geng, D.; Yang, S.; Zhang, Y.; Yang, J.; Liu, J.; Li, R.; Sham, T.-K.; Sun, X.; Ye, S.; Knights, S. Nitrogen doping effects on the structure of graphene. *Appl. Surf. Sci.* **2011**, *257*, 9193.
(37) Wang, H.; Zhang, C.; Liu, Z.; Wang, L.; Han, P.; Xu, H.; Zhang, K.; Dong, S.; Yao, J.; Cui, G. Nitrogen-doped graphene nanosheets with excellent lithium storage properties. *J. Mater. Chem.* **2011**, *21*, 5430.
(38) Galashev, A. E. Structure of water clusters with captured methane molecules. *Russ. J. Phys. Chem. B* **2014**, *8*, 793−800.
(39) Galashev, A. E. Structural changes in water clusters during methane adsorption. *Colloid J.* **2014**, *76*, 300−307.
(40) Le, M.-Q.; Nguyen, D.-T. The role of defects in the tensile properties of silicene. *Appl. Phys. A* **2015**, *118*, 1437.
(41) Kim, K.; Coh, S.; Kisielowski, C.; Crommie, M. F.; Louie, S. G.; Cohen, M. L.; Zett, A. Atomically perfect torn graphene edges and their reversible reconstruction. *Nat. Commun.* **2013**, *4*, 2723.
(42) Bhavadharani, R. K.; Nagarajan, V.; Chandiramouli, R. Silicene nanosheet to discriminate the quality of pear fruit based on volatiles adsorption − a DFT application. *Condens. Matter Phys.* **2019**, *22*, 33001.
(43) Kawahara, K.; Shirasawa, T.; Arafune, R.; Takahashi, T.; Kawai, M.; Takagi, N. Determination of atomic positions in silicene on Ag(111) by low-energy electron diffraction. *Surf. Sci.* **2014**, *623*, 25−28.
(44) Ghadiyali, M.; Chacko, S. Band splitting in bilayer stanene electronic structure scrutinized via first principle DFT calculations. 2019, arxiv: [Cond-mat.mtrl-sci]. https://arxiv.org/pdf/1710.05702.pdf.
(45) Neek-Amal, M.; Sadeghi, A.; Berdiyorov, G. R.; Peeters, F. M. Realization of free-standing silicene using bilayer graphene. *Appl. Phys. Lett.* **2013**, *103*, 261904.
(46) Rademaker, T. J.; Akkermans, G. R. A.; Danilov, D. L.; Notten, P. H. L. On the deviation of electroneutrality in Li-ion battery electrolytes. *J. Electrochem. Soc.* **2014**, *161*, E3365−E3372.
(47) Pan, Y.; Gover, A. Spontaneous and stimulated radiative emission of modulated free-electron quantum wavepackets − semiclassical analysis. *J. Phys. Commun.* **2018**, *2*, 115026.
(48) Pharr, M.; Zhao, K.; Wang, X.; Suo, Z.; Vlassak, J. J. Kinetics of initial lithiation of crystalline silicon electrodes of lithium-ion batteries. *Nano Lett.* **2012**, *12*, 5039−5047.
(49) Persson, K.; Sethuraman, V. A.; Hardwick, L. J.; Hinuma, Y.; Meng, Y. S.; van der Ven, A.; Srinivasan, V.; Kostecki, R.; Ceder, G. Lithium diffusion in graphitic carbon. *J. Phys. Chem. Lett.* **2010**, *1*, 1176−1180.
(50) Yang, F.; Chi, C.; Wang, C.; Wang, Y.; Li, Y. Highly chemoselective reduction of nitroarenesover non-noble metal nickel-molybdenum oxidecatalysts. *Green Chem.* **2016**, *15*, 809−815.
(51) Tersoff, J. Emperical interatomic potential for silicon with improved elastic properties. *Phys. Rev. B: Condens. Matter Mater. Phys.* **1988**, *38*, 9902−9905.
(52) Tersoff, J. Modeling solid-state chemistry: Interatomic potentials for multicomponent systems. *Phys. Rev. B: Condens. Matter Mater. Phys.* **1989**, *39*, 5566−5568.
(53) Galashev, A.; Ivanichkina, K.; Katin, K.; Maslov, M. Computational study of lithium intercalation in silicene channel on a carbon substrate after nuclear transmutation doping. *Computation* **2019**, *7*, 60.
(54) Galashev, A. E.; Elshina, L. A.; Muradymov, R. V. Molecular dynamic study of the mechanism of formation of 2D carbon nanostructures in a solid Al−C nanocomposite grain. *Russ. J. Phys. Chem. A* **2016**, *90*, 2444−2448.
(55) Plimpton, S. Fast parallel algorithms for short-range molecular dynamics. *J. Comp. Phys.* **1995**, *117*, 1−19.


https://dx.doi.org/10.1021/acsomega.0c01240
*ACS Omega* 2020, 5, 13207−13218